Polymer 49 (2008) 5329–5335

Contents lists available at ScienceDirect

Polymer

journal homepage: www.elsevier.com/locate/polymer

High conducting multilayer films from poly(sodium styrenesulfonate) and graphite nanoplatelets by layer-by-layer self-assembly

Qunwei Tang, Jihuai Wu*, Qinghua Li, Jianming Lin

The Key Laboratory for Functional Materials of Fujian Higher Education, Institute of Material Physical Chemistry, Huaqiao University, Quanzhou, Fujian 362021, China

ARTICLE INFO

Article history:
Received 30 May 2008
Received in revised form 15 July 2008
Accepted 6 September 2008
Available online 7 October 2008

Keywords:
Multilayer film
Layer-by-layer self-assembly
Graphite

ABSTRACT

Exfoliated graphite (G) nanoplatelet was modified with hexadecyltrimethylammonium bromide (C_{16}TAB) and was constructed as multilayer films by electrostatic self-assembly. A [poly(sodium styrenesulfonate)/graphite]$_n$ (PSS/G)$_n$ multilayer film was self-assembled by alternate adsorption of polyanionic PSS and cationic graphite nanoplatelets G. An uniform deposition process was detected by UV–vis absorption spectra. The (PSS/G)$_n$ multilayer film exhibits an excellent electrical conductivity in the range of 50–200 S cm^{-1}, when bilayer number (n) exceeds a threshold value four, the conductivity of the multilayer film increases dramatically. Cyclic voltammogram measurement reveals that the (PSS/G)$_n$ film with more bilayer has small charge-transfer resistance and high electrocatalytic activity.

© 2008 Elsevier Ltd. All rights reserved.

1. Introduction

The layer-by-layer (LbL) self-assembly of ultrathin multilayer films from oppositive charged polyelectrolytes and lamellar inorganic particles is a facile, inexpensive and versatile route to multifunctional nano-scaled structures and materials [1–3]. Desired multilayer films have success with sequential LbL constructed onto solid substrates by self-assembly technology. Importantly, unlike the many other methods, self-assembly technique permits the control of the thickness of each layer in the nanometer range [4].

The introduction of inorganic components in multilayer offers optical, electronic, magnetic, mechanical, catalytic, release and sensitive properties that may be difficult to achieve by organic polymers alone [5–8]. Among the various inorganic particles, nano-scaled graphite has attracted more scientific attention for the past decades [9–11]. Graphite is an important conducting material, a peculiarity of graphite is its layered structure formed by parallel two-dimensional graphite sheets weakly coupled by van der Waals interaction. Each graphite sheet looks like a hexagonal network of carbon atoms connected by strong covalent "in-plane" σ–σ bonds [9]. Graphite/polymer composites have been found to possess outstanding physical, chemical, and mechanical properties [4,9,10]. The availability of multilayer films of graphite/polymer composites is an essential requirement for the construction of advanced magnetic, electronic, optical, and electro-optical devices and sensors. For many systems, wet chemical methods have provided a viable approach for composite nanostructured film formation [12].

For the sake of introduction of multifunctional graphite to self-assembly films, modification of the graphite by oxidation (to graphite oxide, GO) has been carried out, which results in the formation of nucleophilic sites (carboxyl or hydroxyl groups) and the interaction with positively charged polyelectrolytes [10,13]. Fendler and co-workers showed that GO could be used for the construction of multilayer films by electrostatic interactions, which could subsequently be reduced electrochemically to make a conducting graphitic film [4,10]. Due to the negative charges on GO, GO/polycation multilayer films were continuously grown with tens of nanometers in their lateral dimensions. A drawback of this method is that only few of carboxyl groups are produced and locate at the edges of the carbon layers on the graphite [13–15], which is difficult to grow multilayer films by electrostatic interactions. To increase the amount of carboxyl groups, it is necessary to increase oxidation degree, whereas the graphite structure will be destroyed and its special properties are suppressed. It is unfavorable to prepare multifunctional multilayer films. Furthermore, using the traditional method, only cationic polyelectrolytes can be assembled with negatively charged GO. The unique polyanions such as poly(acrylic acid) (PAA) and poly(sodium styrenesulfonate) (PSS) cannot be introduced to construct multilayer films consisting of GO.

In the previous work, we reported a novel approach to construct a stable multilayer film by LbL self-assembly PAA and GO nanoplatelets modified with hexadecyltrimethylammonium bromide (C_{16}TAB) [16]. In continuation of our study, a multilayer film from PSS and the graphite (G) nanoplatelets was prepared by LbL self-

* Corresponding author. Tel.: +86 595 22693899; fax: +86 595 22693999.
E-mail address: jhwu@hqu.edu.cn (J. Wu).

0032-3861/$ – see front matter © 2008 Elsevier Ltd. All rights reserved.
doi:10.1016/j.polymer.2008.09.043

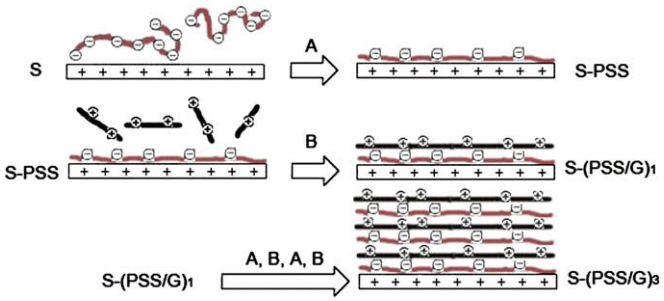

Fig. 1. The self-assembly process of $(PSS/G)_n$ multilayer films. Step A is the deposition of PSS layer; step B is the deposition of $C_{16}TAB$ modified graphite nanoplatelets; by repeating A and B $(PSS/G)_n$ multilayer films are obtained.

assembly technique. Compared with our previous work, owing to GO is reduced to graphite, the conductivity of multilayer film is enhanced. On the other hand, the introduction of PSS with surfactant function and weak hydrophobic property increases the interaction between the polyanion layers of PSS and the oppositive charged layer of the graphite modified with $C_{16}TAB$, the stability of the multilayer is improved. Therefore, a higher conductive and stable $(PSS/G)_n$ multilayer film is LbL self-assembled successfully.

2. Experimental part

2.1. Materials

PSS ($M_w = 70{,}000$) and $C_{16}TAB$ (purity > 99%, CMC = 0.9 mM) were purchased from Aldrich and used without further purification. Graphite powder (an average size of <2 μm, supplied by Shandong Qingdao Graphite Company, China) was used as-received. A modified glass substrate ($2 \times 2\ cm^2$) was obtained as follows: polished glass substrate was sonicated in CCl_4 solution for 30 min and then rinsed with 2-propanol and enough deionized water. The cleaned substrate was immersed in a $C_{16}TAB$ ethanol solution for 2 days and the remaining solvent was evaporated in air.

2.2. Preparation of graphite nanoplatelets modified with $C_{16}TAB$

The pristine graphite powder was vacuum dried at 80 °C for 24 h. Concentrated sulfuric acid and fuming nitric acid ($V_{H_2SO_4} : V_{HNO_3} = 7 : 3$), as oxidizing and intercalating agent were added to expand and oxidize the graphite powder (to GO). Resultant product was heated at 1000 °C and ultrasonic irradiated to exfoliate the expanded GO nanoplatelets. The obtained exfoliated GO nanoplatelets were reduced by hydrazine hydrate for more than 48 h until all hydrophilic groups lost. The graphite nanoplatelet (approximately three carbon layers) was suspended in a $C_{16}TAB$ (0.7 mM) aqueous solution. After a weak agitation for a week, $C_{16}TAB$ was modified on the surface of the graphite nanoplatelet and an even modified graphite suspension thus was obtained. The resulted 0.5 wt% graphite dispersion was used for the assembly of multilayer films.

2.3. Self-assembly of $(PSS/G)_n$ multilayer films

The self-assembly of $(PSS/G)_n$ multilayer film involved the following steps: (A) immersion of the $C_{16}TAB$ modified quartz glass substrate (S) into a 5 mM PSS aqueous solution, kept at pH = 12 for 5 min, rinsing for 1 min with enough amount of deionized water, thus a film of S-PSS was obtained; (B) immersion the film S-PSS into a 0.5 wt% modified graphite suspension for 15 min, washing with enough amount of deionized water, thus an S-$(PSS/G)_1$ film was obtained. Each washing was followed by drying in a stream of N_2 gas for 1 min. A subsequent bilayer number (n) of sandwich layers, to produce a multilayer film containing alternating n layers of PSS and n layers of graphite, S-$(PSS/G)_n$, were prepared by repeating steps A and B n times as shown in Fig. 1.

2.4. Characterization and measurement

Fourier transform infrared (FTIR) spectra of samples were identified by mixing the sample with solid KBr, grinding, pressing into a pellet and measuring with a Nicolet Impact 410 FTIR spectrophotometer. The growth of the sequence $(PSS/G)_n$ was monitored by measuring the UV–vis characteristic absorption bands at 225 nm and 260 nm for PSS and graphite [17] with Shimadzu UV-3100 UV–VIS–IR spectrophotometer. Atomic force microscopy (AFM) images of samples were observed with an NS3A-02 Nanoscope III and using scanning probe microscope (Veeco Co.) in tapping mode.

Electrochemical measurements of the film samples were performed with a three-electrode electrochemical cell using a CHI660C potentiostat. Cyclic voltammetry was carried out in a N_2 purged acetonitrile solution. The $(PSS/G)_n$ film electrode was used as working electrode, respectively. A Pt coil as the counter electrode and an Ag/AgCl electrode as reference electrode were used. The electrolyte was the acetonitrile solution containing 0.1 M $LiClO_4$ as the supporting electrolyte and 10 mM LiI, 1 mM I_2 as the redox couple. In acetonitrile medium, I_2 and I^- integrate to I_3^- ions ($I_2 + I^- = I_3^-$), which are an oxidized state of iodide and can capture electrons to form I^- ions.

In order to study the stability of $(PSS/G)_n$ multilayer films under UV irradiation, the irradiation experiment was carried out using a 300 W high-pressure mercury lamp as UV light source. The (PSS/

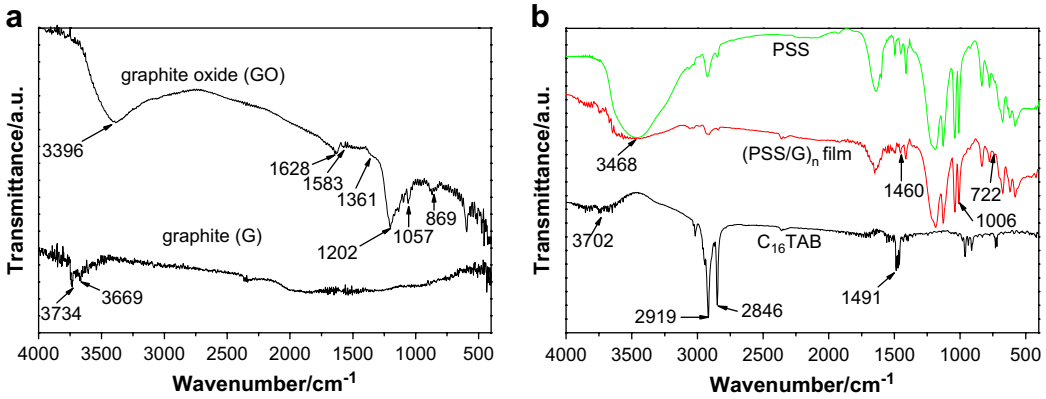

Fig. 2. FTIR spectra of (a) graphite oxide and graphite nanoplatelets; (b) $C_{16}TAB$, PSS and $(PSS/G)_{12}$ multilayer film.

G)$_n$ multilayer film was settled on a level platform, after a given time irradiation, the absorbance at 225 nm and conductivity of the film were measured, and the ATM image was observed, which is useful to study the stability of (PSS/G)$_n$ multilayer films under UV irradiation.

3. Results and discussion

3.1. FTIR spectra

In the FTIR spectrum of GO (Fig. 2a), the broad band centered at 3396 cm^{-1} is attributed to O–H stretching vibration of the C–O–H groups. The band at 1628 cm^{-1} is assigned to C=O stretching vibrations of the carbonyl and carboxyl groups. Absorption bands at 1361 and 1583 cm^{-1} are the results of O–H deformations of C–O–H groups and water, respectively. The bands at 1057 and 1202 cm^{-1} are due to C–O (i.e., hydroxyl, ether) stretching vibrations. The absorption bands below ~1000 cm^{-1} are due to the presence of trace sulfate groups by H_2SO_4 intercalated between graphite planes, or possibly as the free acid [18]. After reduction by hydrazine hydrate for more than 24 h, all the groups disappear except the O–H stretching locating at 3734 and 3669 cm^{-1}, which indicates that the GO nanoplatelet has been reduced to graphite and facilitate the increase of conductivity of the multilayer films. The conductivity of initial graphite powder is 2500 S cm^{-1}, after the exfoliation to GO nanoplatelets, the conductivity decreases to 16.5 S cm^{-1}. In fact, the conductivity of reduced graphite nanoplatelets reaches more than 500 S cm^{-1}, although lower than that of pristine graphite powder, enough to construct high conducting (PSS/G)$_n$ multilayer films.

The FTIR spectra of the C_{16}TAB, PSS and (PSS/G)$_n$ multilayer film are shown in Fig. 2b. The broad band with a center at 3702 cm^{-1} responding to –NH_2 asymmetrical stretching vibration shifts to around 3468 cm^{-1} in the self-assembly film. The absorption peaks at 2919, 2846 and 1491 cm^{-1} attributed to C–H asymmetrical stretching, symmetrical stretching and bending vibrations, respectively, are weakened in (PSS/G)$_{12}$ film. The band corresponding to C–N stretching in C_{16}TAB shifts to 1006 cm^{-1} after the interactions with oppositive charged PSS. The shift of characteristic bands indicates that strong interactions between C_{16}TAB arrays and PSS segments are present. The absorption band at 1460 cm^{-1} is due to –CH_2 deformation and is weakened in the other two spectra. Band at 722 cm^{-1} is the result of –$(CH_2)_n$–CH_3 in-plane rocking and disappears after the formation of C_{16}TAB arrays in graphite nanoplatelets. The above two unconventionalities are caused by the ordered arrangement of C_{16}TAB on hydrophobic graphite surfaces, which restricts rocking and deformation of the tails. Due to the undetected vibration bands in reduced graphite, the spectrum of (PSS/G)$_n$ indicates a strong attraction of C_{16}TAB arrays with PSS chains and hydrophobic interaction with graphite surfaces [19].

3.2. Bilayer number and deposition time of (PSS/G)$_n$

UV–vis spectra have been fruitfully employed for monitoring the LbL growth of sequentially adsorbed polyelectrolytes and a variety of different building blocks [20–22]. Fig. 3 shows the UV–vis absorption spectra of (PSS/G)$_n$ films with $n = 2$–12. The PSS and graphite have characteristic absorption peak at 225 nm and 260 nm [17], respectively, which is used to monitor the growth of the layers and the assembly process of the (PSS/G)$_n$ films. It is notable that a freshly prepared GO has a sensitive absorption peak at 236 nm, however, the absorption band at 236 nm does not appear in the UV–vis absorption spectra of (PSS/G)$_n$ films, which further indicates that GO has been reduced to graphite. The absorbance at the 260 nm and 225 nm increases linearly with the numbers of the attached PSS and graphite layers in the film (inset of Fig. 3), which indicates a progressive and uniform deposition process of the (PSS/G)$_n$ multilayer and suggests the amounts of absorbed PSS and graphite in the assembly process are essentially the same for each layer.

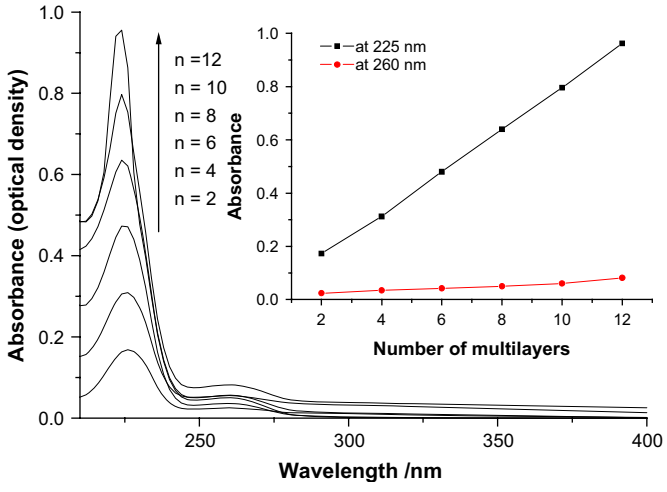

Fig. 3. UV–vis absorption spectra of (PSS/G)$_n$ films with $n = 2$–12. The inset shows plots of absorbances at 225 nm and 260 nm against n.

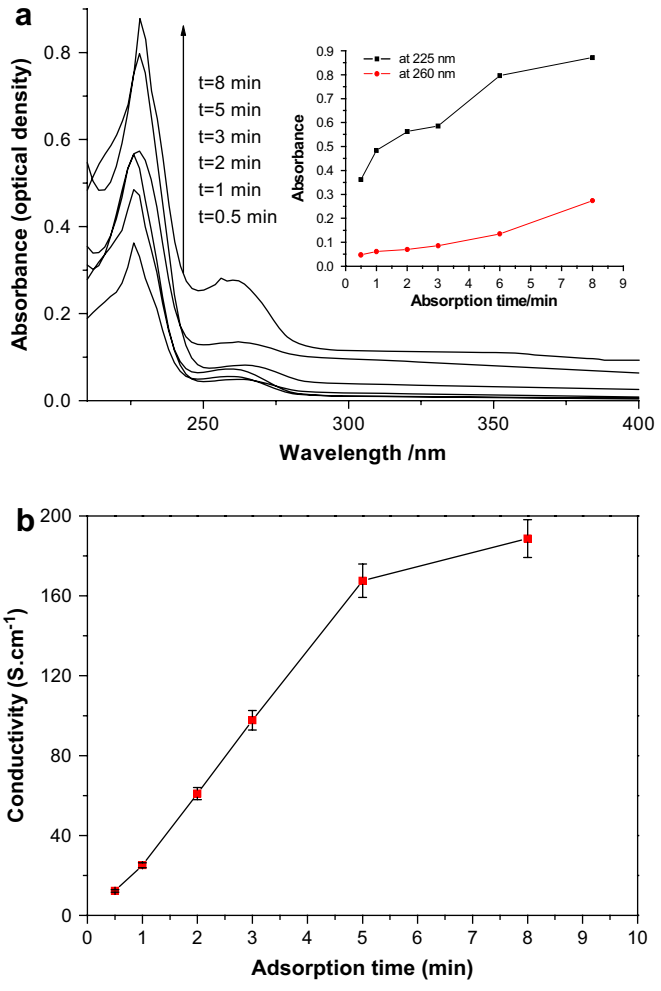

Fig. 4. (a) UV–vis absorption spectra of (PSS/G)$_{10}$ multilayer films at different PSS deposition time; (b) conductivity of (PSS/G)$_{10}$ multilayer film at different PSS deposition time (the deposition time at G colloids is fixed at 15 min).

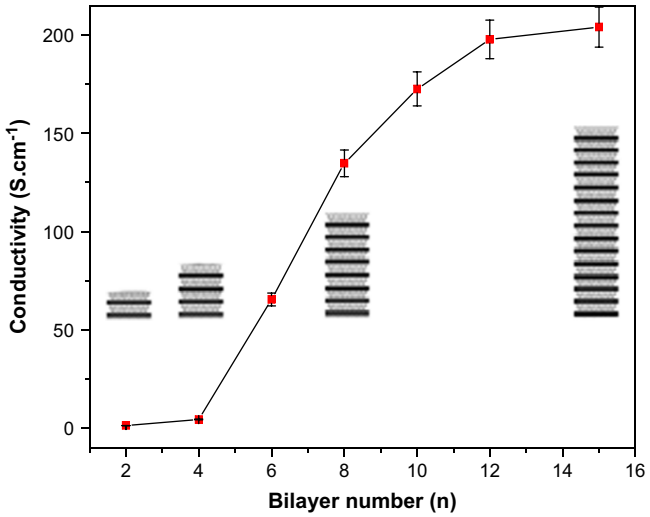

Fig. 5. Conductivities of $(PSS/G)_n$ films as a function of the deposition cycle.

The absorbance of a series of PSS layers deposited on graphite layers at different deposition times is determined as shown in Fig. 4(a). It can be seen that the adsorption of PSS is rather fast and nearly reaches saturation within 5 min. Also, from the conductivity of $(PSS/G)_{10}$ multilayer film at different PSS deposition time shown in Fig. 4(b), the conductivity of the (PSS/G) reaches a higher value within 5 min. The results are accord with the absorption spectra in Fig. 4(a).

The adsorption of PSS and C_{16}TAB modified graphite can be explained by ion-exchange model [23]. Due to the entropy effect by adsorbing PSS and C_{16}TAB modified graphite and the neutralization by small monovalent ions (Na^+ and Br^- ions) on the surface of the films, the oppositive charged components cannot be unrestrictedly adsorbed. Equilibrium adsorption is not obtained until the adsorbed PSS molecules or cationic graphite nanoplatelets are electrostatically repelled from the surface. In our experiments, the adsorption time of PSS was controlled for 5 min, and that of C_{16}TAB modified graphite colloid to be 15 min.

3.3. Electrical conductivity

The dependence of the conductivity of $(PSS/G)_n$ multilayer films on the deposition cycle is shown in Fig. 5. It can be seen that the conductivity is very low at $n < 4$, whereas increases dramatically at $n > 4$. For example, the conductivities of $(PPS/G)_n$ at $n = 1$ and 4 are 1.2 and 4.3 S cm^{-1}, respectively. Once n increases from 4 to 12, the conductivity dramatically increases from 4.3 S cm^{-1} to 197.8 S cm^{-1}. With the further increase of deposition cycles to 15, the conductivity of the multilayer film is 204.1 S cm^{-1}.

In the case of conventional polymer/graphite composites, the abrupt increase of conductivity is designated a percolation phenomenon and the transition point is percolation threshold. According to the percolation theory, once the dosage of graphite in composites reaches a percolation threshold value, the conductivity of the composite will dramatically increase as a result of the connection of conducting channels. In the case of $(PSS/G)_n$ multilayer films, graphite and PSS are in linear increase with increasing of deposition cycles, in other words, the graphite content has an approximate percentage relative to PSS. And due to the relation of conductivity to n, instead of the percentage of conducting component graphite nanoplatelets, the phenomenon cannot be explained by the percolation theory. In our previous

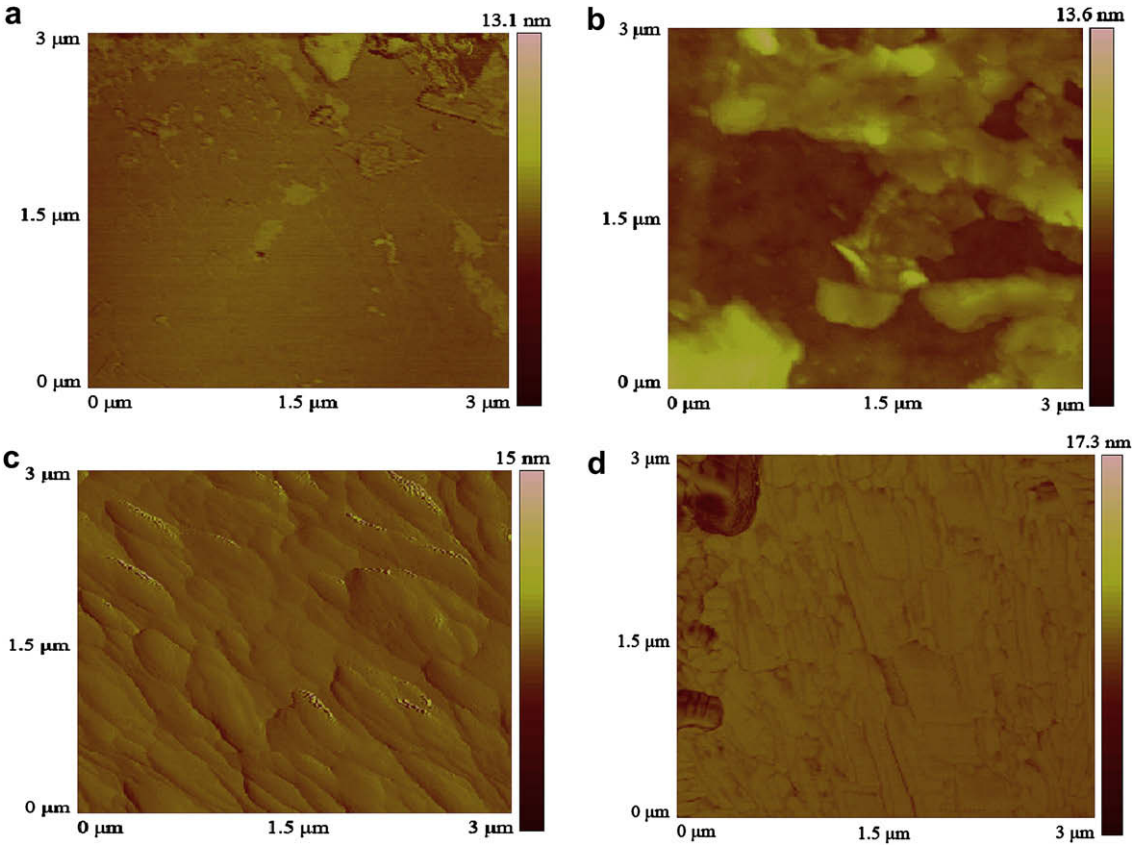

Fig. 6. AFM images of the graphite terminated $(PSS/G)_n$ multilayer films with different n values. (a) $n = 1$, (b) $n = 4$, (c) $n = 12$, (d) $n = 15$.

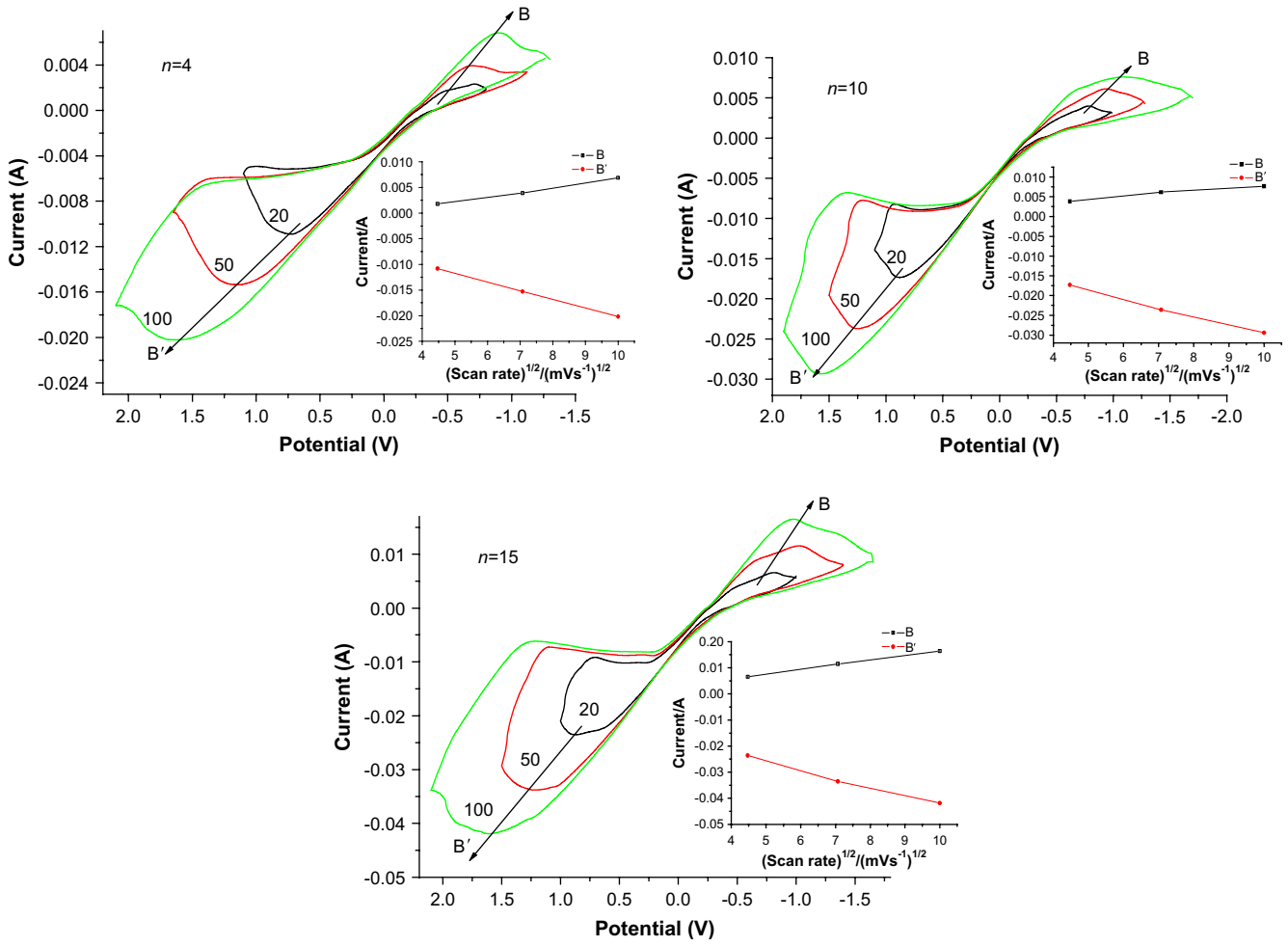

Fig. 7. Cyclic voltammograms for the $(PSS/G)_n$ multilayer films with different bilayer numbers in acetonitrile solution of 0.1 M $LiClO_4$, 10 mM LiI, 1 mM I_2 with different scan rates (from inner to outer: 20, 50, and 100 mV s^{-1}, respectively). The insets are in linear relationship between all the redox peak currents and square root of scan rates.

work [16], we explained the phenomenon from the view of electron transfer in the carbon interlayer of the graphite oxide nanoplatelets. The increasing of C–C interlayer distance between carbon layers in each GO sheet loosened the astriction of carbon layer to electrons in the interlayers and improved the electron transfer. When the C–C interlayer height reached a threshold value (or n reached a threshold value), the electrons in the carbon interlayer became free, and the conductivity of the films increased sharply. Similar explanation beseems the $(PSS/G)_n$ multilayer film in this paper. According to above experimental results, the charge threshold value (n_t) for the $(PSS/G)_n$ multilayer film is four.

Fig. 6 shows the AFM images of the graphite terminated $(PSS/G)_n$ multilayer films with $n = 1$, 4, 12, and 15. As an example, the image of the graphite terminated S-$(PSS/G)_1$ monolayer film (Fig. 6a) is discussed. The height of the S-$(PSS/G)_1$ monolayer consists of doubled C_{16}TAB length (the C_{16}TAB arrays on two surfaces of a graphite nanoplatelet), one PSS thickness and one graphite thickness. The C_{16}TAB molecules are oriented perpendicular to graphite plane, with the hydrophilic head groups completely shielding the hydrophobic graphite from solution [24]. The length of an extended C_xTAB molecule in the all-trans conformation of the alkyl chain is given by Eq. (1)

$$l(C_xTAB) = 0.245\left(\frac{x}{2} - 1\right) + r_{Me} + r_{N-Me} \quad (1)$$

where the van der Waals radius of the methyl (r_{Me}) is 0.2 nm, and the van der Waals radius of the trimethylammonium end groups (r_{N-Me}) is 0.35 nm [25,26]. This formula yields $l = 2.27$ nm for C_{16}TAB in a zigzag conformation. The thickness of G layer and PSS layer is approximately 4.4 and 4.1 nm, respectively [16,4,27]. So, the total thickness of S-$(PSS/G)_1$ monolayer is $d_1 = 2.27 \times 2 + 4.1 + 4.4 = 13.0$ nm, which is nearly consistent with AFM observation in Fig. 6a. The slight deviation originates from the fact that the self-assembly technique yields the average thickness of the presumed uniform film.

From Fig. 6, it also can be seen that with the bilayer number (n) increases from 1 to 4, 12 and 15, the terminated bilayer height increases from 13.1 to 13.6, 15.0 and 17.3 nm. The increase of bilayer height means the expanding of the C–C interlayer of graphite nanoplatelets and the increase and the conductivity of the $(PSS/G)_n$ film, which is consistent with Fig. 5.

Table 1
Peak currents of the $(PSS/G)_n$ multilayer films at different scan rates and bilayer numbers.

Scan rate (mV s^{-1})	Peak current (mA, $n = 4$)		Peak current (mA, $n = 10$)		Peak current (mA, $n = 15$)	
	B	B'	B	B'	B	B'
20	1.81	−10.84	3.86	−17.31	6.56	−23.63
50	3.90	−15.28	6.15	−23.58	11.49	−33.57
100	6.89	−20.16	7.69	−29.39	16.42	−41.82

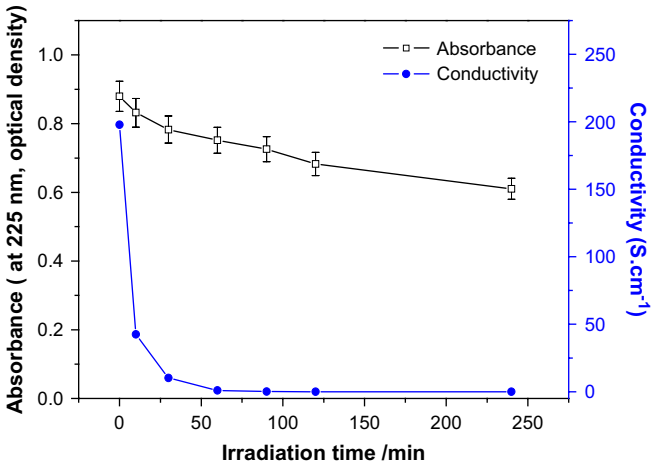

Fig. 8. The absorbance at 225 nm and conductivity of $(PSS/G)_{12}$ multilayer film under UV irradiation.

3.4. Electrochemical properties

$(PSS/G)_n$ multilayer films are expected to be a counter electrode used in dye-sensitized solar cell [28,29]. The cyclic voltammograms of the LiI/I_2 system on the $(PSS/G)_n$ multilayer film electrodes at different scan rates are measured and shown in Fig. 7. It can be found that the absolute values of cathodic peak currents are the almost same as those of the corresponding anodic peak currents. The cathodic peak gradually and regularly shifts to the negative direction and the corresponding anodic peak shifts to the positive direction with increasing scan rate. By plotting the cathodic and anodic peak currents against the square root of the scan rate, the good linear relationship with various scan rates indicates the diffusion limitation of the redox reaction on $(PSS/G)_n$ multilayer film electrode [30,31]. This phenomenon suggests that there is no specific interaction between I_2/I^- redox couple and $(PSS/G)_n$ multilayer film electrode [30,32].

To quantify the intrinsic relations of redox of the $(PSS/G)_n$ multilayer films at different scan rates and deposition cycles, the peak currents at scan rates of 20, 50, 100 mV s^{-1} and bilayers of 4, 10, 15 are shown in Table 1. It can be seen that the films with higher bilayers have considerable higher redox current than those with lower ones. The difference in the redox currents results from the conductivity of $(PSS/G)_n$ multilayer films. As discussed in the Section 3.3, the $(PSS/G)_n$ multilayer film with higher n value has a higher conductivity, which means lower electrical resistance and higher redox currents as a electrode. On the other hand, the films with more deposition cycles have the highest effective surface area, which is desirable for high efficiency and sensitivity of many devices. This suggests a faster reaction rate on the higher bilayer film electrodes than that on the lower ones. In other words, the charge-transfer resistance for the I_2/I^- redox reaction is smaller on the higher bilayer film electrodes compared with

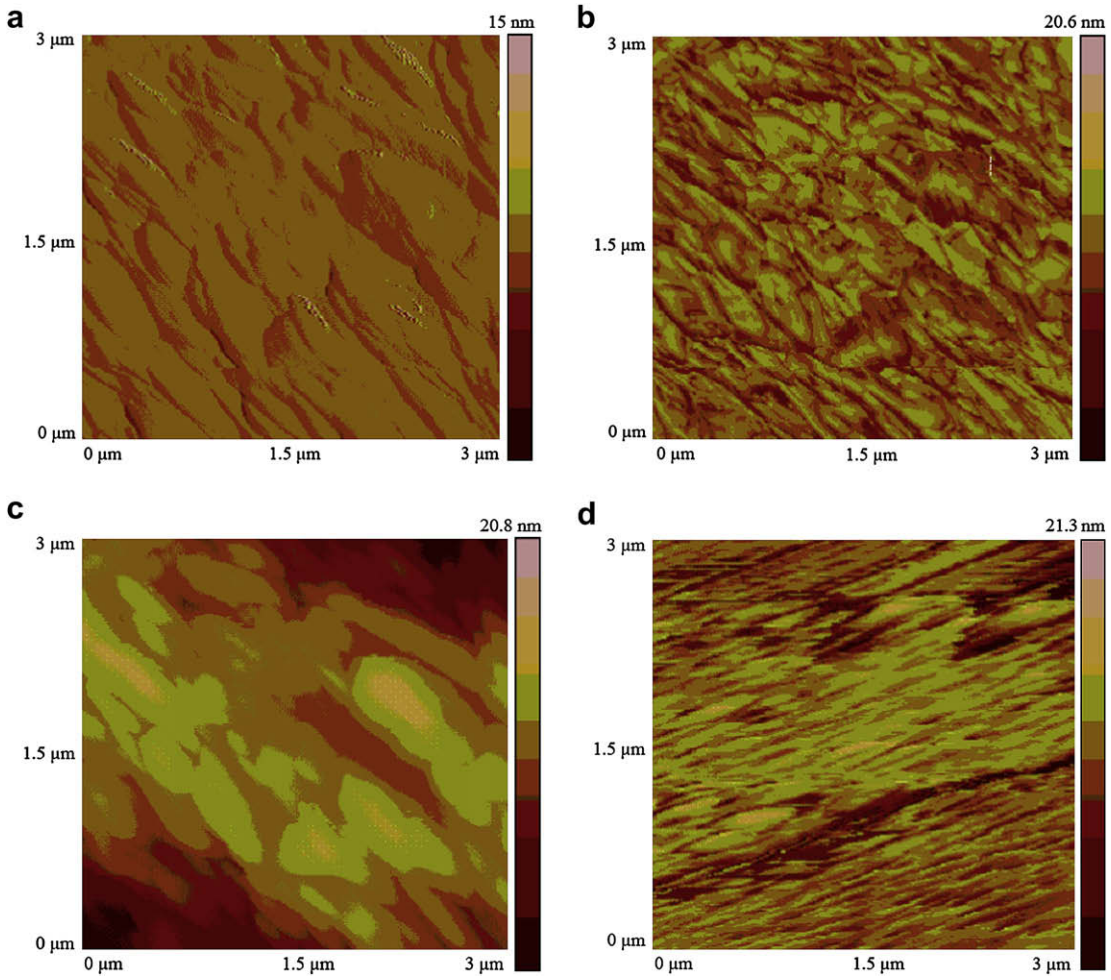

Fig. 9. AFM images of $(PSS/G)_{12}$ multilayer film after (a) 0 min, (b) 10 min, (c) 30 min, and (d) 240 min UV irradiation, respectively.

lower ones under the same conditions [33]. As more layers are deposited, the electron transfer is dominated by the counterion diffusion into the film (perchlorate and iodide anions in this case), thus causing the diffusional behavior in the cyclic voltammograms.

3.5. UV irradiation stability

Fig. 8 shows the absorbance and conductivity of $(PSS/G)_{12}$ multilayer film under UV irradiation. After 10 min, 30 min, and 240 min irradiation, the absorbency at 225 nm of $(PSS/G)_{12}$ multilayer film is 94.6%, 89.1%, and 69.4% of the original absorbance, and the conductivity decreases from 197.8 S cm^{-1} to 12.5, 10.2 and 1.05 S cm^{-1}. From the irradiated AFM images shown in Fig. 9, it can be seen that the surface of the $(PSS/G)_{12}$ film becomes rough and undulate after 10 min UV irradiation, which indicates the decomposition of PSS and even C_{16}TAB, the connective graphite nanoplatelet network also collapses. When the irradiation time is 30 min, the graphite nanoplatelets are bare. It may be due to the gradual decomposition of PSS layers from the surface to the inner after the complete decomposition of PSS in the twelfth bilayer. Once the irradiation time is prolonged to 240 min, a porous surface is observed without graphite nanoplatelets. In this case, the polyelectrolyte segments are nearly all decomposed and the conductivity decreases to 0.025 S cm^{-1}. The graphite nanoplatelets are adsorbed on PSS layers by electrostatic interactions. Under the deep collapse of organic compounds, such as C_{16}TAB and PSS, the charged groups, including sulphonic ($-SO_3^-$) and quaternary amine ($>N^+<$) groups have been lost and the electrostatic interactions are broken. Thus, the adsorbed graphite nanoplatelets peel off the system, the released carbon dioxide and other gases diffuse from the matrix, which results in the formation of porous structure.

4. Conclusions

$(PSS/G)_n$ multilayer films were LbL self-assembled from exfoliated graphite nanoplatelets and PSS. The FTIR spectra offered an evidence for the strong interaction between PSS and the C_{16}TAB/G system. The growth of the films was detected by UV–vis spectra, showing an uniform deposition process of the $(PSS/G)_n$ multilayer films. The $(PSS/G)_n$ multilayer film exhibits an excellent electrical conductivity in the range of 50–200 S cm^{-1}, when bilayer number (n) exceeds a threshold value four, the conductivity of the multilayer film increases dramatically, which maybe due to that the electrons in the carbon interlayer became free, when the C–C interlayer height reached a threshold value (or n reached a threshold value). Cyclic voltammograms of I_2/I^- system measurement revealed the $(PSS/G)_n$ multilayer film with more bilayers has small charge-transfer resistance and high electrocatalytic activity. Properties of these multilayer films render them potential applications for the construction of components of advanced optical and electronic devices.

Acknowledgement

The authors thank for jointly support by the National Natural Science Foundation of China (No. 50572030), the Specialized Project of Fujian Province (No. 2005HZ01-4, No. 2007HZ0001-3), the Key Project of Chinese Ministry of Education (No. 206074) and Specialized Research Fund for the Doctoral Program of Chinese Higher Education (No. 20060385001).

References

[1] Fendler JH. Chem Mater 1996;8(8):1616–24.
[2] Whitesides GM, Mathias JP, Seto CT. Science 1991;254:1312–9.
[3] Ulbricht M. Polymer 2006;47(7):2217–62.
[4] Kotov NA, Dekany I, Fendler JH. Adv Mater 1996;8(8):637–41.
[5] Zhang TZ, Ge LQ, Wang X, Gu ZZ. Polymer 2008;49(12):2898–902.
[6] Li CY, Wen TC, Guo TF, Hou SS. Polymer 2008;49(4):957–64.
[7] Egawa Y, Hayashida R, Anzai JI. Polymer 2007;48(6):1455–8.
[8] Lu XL, Cheng I, Mi YL. Polymer 2007;48(3):682–6.
[9] Obraztsov AN, Obraztsova EA, Tyurnina AV, Zolotukhin AA. Carbon 2007;45(10):2017–21.
[10] Cassagneau T, Fendler JH. Adv Mater 1998;10(11):877–81.
[11] Cassagneau T, Guerin F, Fendler JH. Langmuir 2000;16(18):7318–24.
[12] Fendler JH. Membrane-mimetic approach to advanced materials. In: Advances in polymer science, vol. 11. Springer; 1994. p. 3.
[13] Kovtyukhova NI, Ollivier PJ, Martin BR, Mallouk TE, Chizhik SA, Buzaneva EV, et al. Chem Mater 1999;11(3):771–8.
[14] Szabo T, Tombacz E, Illes E. Carbon 2006;44(3):537–45.
[15] Scholz W, Boehm HP. Z Anorg Allg Chem 1969;369(3–6):327–40.
[16] Wu JH, Tang QW, Sun H, Lin JM, Ao HY, Huang ML, et al. Langmuir 2008;24(9):4800–5.
[17] Xu L, Zhang HY, Wang EB, Kurth DG, Li Z. J Mater Chem 2002;12(3):654–7.
[18] Szabo T, Szeri A, Dekany I. Carbon 2005;43(1):87–94.
[19] Schoeler B, Kumaraswamy G, Caruso F. Macromolecules 2002;35(3):889–97.
[20] Cassagneau T, Fendler JH. J Phys Chem B 1999;103(11):1789–93.
[21] Chirea M, Pereira CM, Silva F. J Phys Chem C 2007;111(26):9255–66.
[22] Ghannoum S, Xin Y, Jaber J, Halaoui LI. Langmuir 2003;19(11):4804–11.
[23] Li XF, Zhao S, Yang M, Sun CQ, Guo LP. Thin Solid Films 2005;478(1–2):310–7.
[24] Manne S, Cleveland JP, Gaub HE, Hansma PK. Langmuir 1994;10(12):4409–13.
[25] Pauling L. The nature of the chemical bond. Ithaca, NY: Cornell University Press; 1960. p. 261.
[26] Kiraly Z, Findenegg GH. J Phys Chem B 1998;102(7):1203–11.
[27] Stockton WB, Rubner MF. Macromolecules 1997;30(9):2717–25.
[28] Wu JH, Li QH, Fan LQ, Lan Z, Lin JM, Li PJ, et al. J Power Sources 2008;181(1):172–6.
[29] Li QH, Wu JH, Tang QW, Li PJ, Lan Z, Lin JM, et al. Electrochem Commun available online 5 July 2008.
[30] Saito Y, Kubo W, Kitamura T, Wada Y, Yanagida S. J Photochem Photobiol A 2004;164(1–3):153–7.
[31] Biallozor S, Kupniewska A. Electrochem Commun 2000;2(7):480–6.
[32] Hauch A, Georg A. Electrochim Acta 2001;46(22):3457–66.
[33] Andrieux CP, Saveant JM. J Electroanal Chem 1980;111(2):377–81.